Current-Induced Light Modulation Using Quantum Wells in the Collector of Heterojunction Bipolar Transistors

Nachum Shamir, Dan Ritter, and David Gershoni

Abstract—We incorporated InGaAs quantum wells within the collector of InP-based heterojunction bipolar transistors to form novel light-modulating devices. We studied the properties of these devices as light modulators by direct current injection. The devices were characterized using differential photocurrent and transmission spectroscopies. Our results demonstrate the feasibility of light modulation based on current rather than electric field modulation. Maximum modulation is achieved when the accumulated carriers quench the excitonic absorption resonance.

Index Terms—Electroabsorption, heterojunction bipolar transistors (HBTs), optical modulation, optical spectroscopy, quantum-well (QW) devices.

I. INTRODUCTION

MULTIPLE-QUANTUM-WELL (MQW) light modulators based on electric field modulation or the quantum confined Stark effect (QCSE) are widely used and well understood [1], [2]. A different approach for light modulation based on charge displacement is known as the barrier reservoir and QW electron transfer (BRAQWET) structure. The latter concept is based on absorption modulations by field-induced accumulation and removal of carriers from the barriers to the QWs and back [3]–[6]. Both types of modulators, though different in concept, are voltage-driven and hence require driver circuits capable of providing relatively high voltage at high speed. In this study, we demonstrate an alternative approach, in which the absorption is modulated and controlled by the collector current of a heterojunction bipolar transistor (HBT). The integrated transistor-modulator is operated in the common base configuration, in which high-frequency current modulation can be achieved. The advantage of the proposed device is in the combined use of voltage and electric current. Small voltage changes at the collector significantly affect the carrier confinement and can be used for rapid depletion of the wells. We believe that by optimizing the collector structure and operating conditions one could speed up the device and obtain useful operation frequencies at lower voltages compared to standard modulation devices.
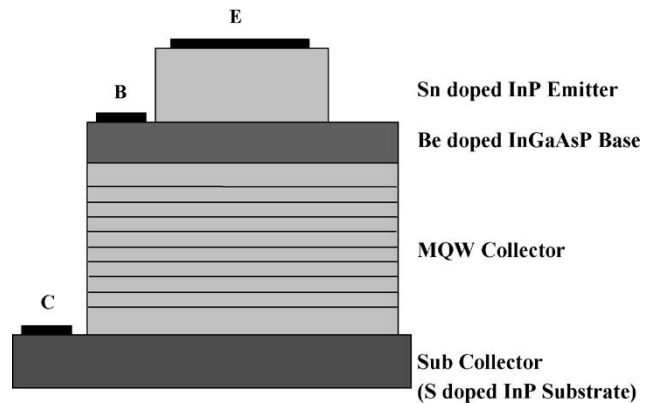
Fig. 1. Schematic description of the MQW HBT structure.

We used photocurrent and transmission spectroscopy to study the feasibility of this novel concept. Our study conclusively demonstrates that this concept works, and we suggest possible ways for improving the modulation efficiency.

II. DEVICE STRUCTURE AND EXPERIMENTAL SETUP

In Fig. 1, we show the structure of the HBT-modulator device. The device layers were grown by a compact metalorganic molecular beam epitaxy (MOMBE) system [7], on a (100)-oriented substrate, with Be and Sn as P and N type dopants, respectively. The lattice-matched InGaAs QW width was designed for effective light modulation at $\lambda = 1.55$ μm. In order to minimize light absorption in the transistor base a quaternary $In_{0.72}Ga_{0.28}As_{0.61}P_{0.39}(\lambda = 1.3$ μm$)$ layer composition was used. The redistribution of beryllium in the InP–InGaAsP HBTs limited the maximum doping level in the base to about $1*10^{19}$ cm^{-3} [8]. Large area (emitter size $20*90$ μm) test devices were fabricated by conventional wet etching. Pt–Ti–Pt–Au contacts were deposited by e-beam evaporation and defined by a lift-off technique.

The band diagrams of the base collector layers as obtained by numerical solutions of the Poisson equations for the three types of devices that we studied are shown in Fig. 2. Devices A and C are single heterojunction transistors, whereas device B is a double heterojunction device with an $In_{0.85}Ga_{0.15}As_{0.33}P_{0.67}(\lambda = 1.1$ μm$)$ grading layer. The grading layer reduced the turn on voltage of the transistor to allow low-voltage operation. Device C is similar to A with the addition of thin InP barriers adjacent to each QW in order
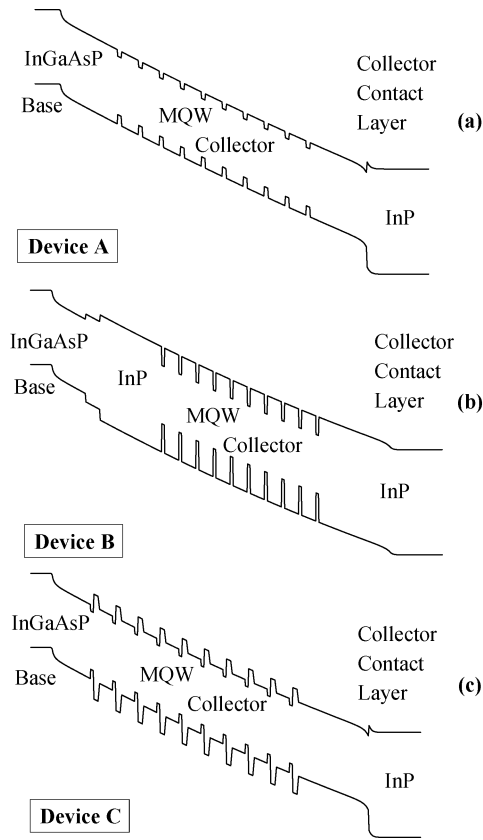
Fig. 2.   Base collector band diagrams, obtained by a numerical solution of the Poisson equation, for devices (a) A, (b) B, and (c) C. Device A has a homogeneous base collector junction. Device B has a graded composite collector, and device C has a homogeneous base collector junction and thin InP barriers to enhance the electron tapping and confinement.

to enhance the electron trapping efficiency. The background doping level of the collector layers was about 1×10^{16} cm^{-3}.

We characterized the various devices using photocurrent and transmission spectroscopy methods. The experimental setups are schematically described in Fig. 3. For photocurrent measurements, the base collector junction was reversely biased in an open emitter configuration, a mechanical chopper modulated the incident light, and the photocurrent part was separated from the total base collector junction current by a lock-in amplifier [Fig. 3(a)].

For transmission modulation measurements, we backside-illuminated the devices through the InP substrate. The transmitted light was reflected by the front metal contacts, thus doubling the absorption of light in the modulator. The reflected light was directed onto our Germanium detector by a beam splitter [Fig. 3(b)]. For these measurements, the transistors were operated in the common base mode. The modulations in the intensity of the reflected light induced by the collector current and voltage changes were measured using a standard lock-in technique.

Current changes cause parasitic voltage changes, due to the resistance of the base layer. In order to separate the current-induced absorption from that induced by voltage changes, we also measured the reflected light modulation under direct modulation of the base–collector junction voltage using a 400-mV ac

signal superimposed on the dc voltage. We identified the true current-induced modulations by comparison between the two independent measurements.

The light- and heavy-hole excitonic absorption resonances were clearly observed by photocurrent spectroscopy in all the devices even at room temperature (Fig. 4). This indicates relatively sharp interfaces and low background doping. Under moderate reverse bias, the heavy-hole exciton resonance shifts toward lower energies as expected from the QCSE [1], [2]. For yet higher bias, depending on the device, the resonance broadens and eventually disappears. We note that the quenching of the heavy-hole resonance in device A occurs at lower reverse bias than that in devices B and C. This is probably due to weaker confinement of the electronic wave function by the quaternary barriers. In the following, we therefore discuss only measurements performed on devices B and C, which performed much better than device A.

III. CURRENT-INDUCED ABSORPTION MODULATION SPECTROSCOPY

The current-induced modulation spectra of devices B and C are presented in Fig. 5 where they are also compared with the voltage-induced modulation spectra. The detector phase was set to produce positive modulation signals when the absorption increase correlated to the current or voltage increase. The current induced signal is clearly visible in the spectra of device B [Fig. 5(a)] at low reverse bias voltage of the base-collector junction. The signal decreases for higher reverse bias levels, probably due to the depletion of carriers from the wells and reduction of the electron confinement efficiency.

The structural design of device C results in better carrier collection efficiency. This is clearly evident from the much lower collector currents of 20 μA ($\sim$ 1 A/cm^2) that are required for observing current-induced modulations similar to these observed for device B at 1 mA ($\sim$ 50 A/cm^2). These spectra are presented in Fig. 5(b), where the current-induced HH1 and LH1 excitonic resonances are observed at low bias. At higher bias levels, these current-induced peaks are reduced due to the lower density of carriers in the wells. The additional spectral features in Fig. 5(a) are due to the HH2 and LH2 excitonic resonances associated with the marginally bounded E2 level. We believe that these spectral features in Fig. 5(b) are associated with the E2 continuum miniband [9]–[11].

It has been previously demonstrated that optical interference alters the phase of the photoreflection signals [12]. We assumed that in our measurements the phase was not altered due to the use of direct electrical modulation. To increase our confidence, we repeated the voltage modulation measurements focusing the light on the inactive collector area, below the base contact. In the second measurement, the light was reflected by the base contact, forming an optical path that did not include the emitter layers. In the two measurements, we obtained similar voltage modulation signals. In addition, we measured several devices, located on remote locations in the sample. In all, we received similar modulation signals and did not observe any influence of the optical path through the sapphire holder, glue, and hand-polished
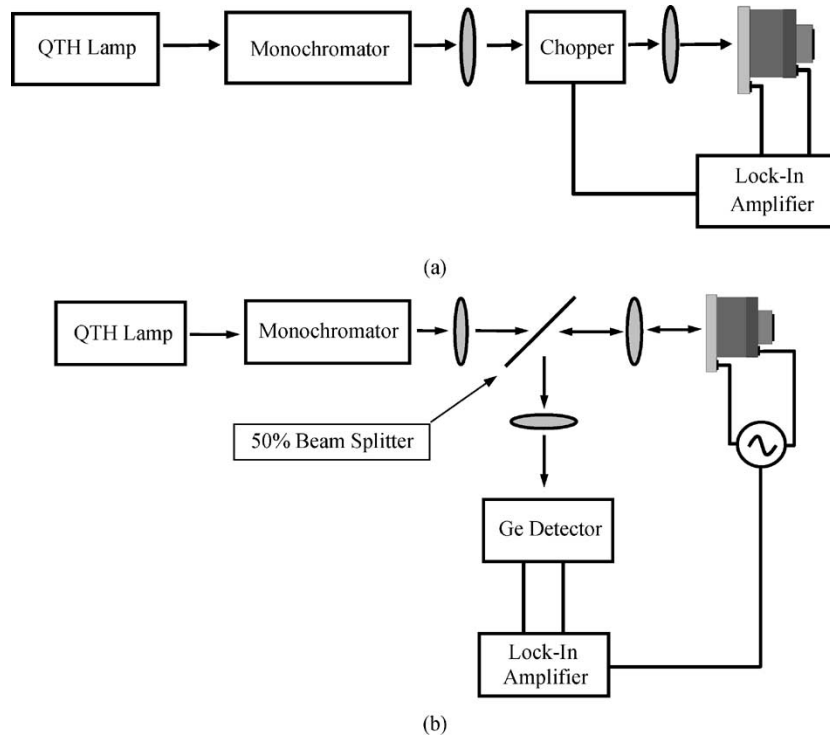
Fig. 3. Schematic description of the experimental setup (a) for photocurrent spectroscopy and (b) for current and voltage induced transmission spectroscopy. In the first mode, the light is modulated and the differential photocurrent is detected by the lock-in amplifier. In the second mode, the collector current or voltage are modulated and the detector and lock-in amplifier measure the differential transmission.

substrate. Interference effects observed in wide-spectral-range photocurrent measurements (not presented) indicated that the optical paths were different for each device.

IV. DISCUSSION

The current-induced absorption modulation spectra are better understood by comparison to the photocurrent spectra. We first discuss the absorption modulation spectrum obtained by modulation of the base collector voltage keeping the emitter open, i.e., with no current injection into the collector. This spectrum is shown in Fig. 6 together with the photocurrent spectrum, both measured for device C at 77 K. Two plots are presented, the first at zero dc bias [Fig. 6(a)], and the second [Fig. 6(b)] at a reverse bias of 2 V. In both cases, the voltage modulation amplitude was 400 mV. A marked difference between the two absorption modulation spectra can be seen: the zero bias spectrum is negative at the absorption edge, while the 2-V bias curve is positive at the absorption edge. Understanding this observation is crucial for the understanding of the current-induced effects, as explained below. While at zero bias, there is a residual density of carriers in the QWs, due to background doping and thermal activation; at reverse bias, the QWs are fully depleted. Thus, at zero bias, the voltage modulation spectrum results from modulation of the residual carrier density. These carriers quench and broaden the excitonic absorption resonance, screen the built-in field and induce bandgap-narrowing effects [3], [13]. The trapped carrier concentration is reduced when the reverse bias increases. The negative signal at the band edge [region (1) in Fig. 6(a)] and the positive peak [region (2)] at the wavelength of the heavy-hole exciton resonance indicate a blue shift of the absorption edge

due to the field-induced carrier depletion with the voltage increase.

The QWs are completely depleted with the reverse bias increase. In Fig. 6(b), we compare photocurrent and voltage modulation spectra measured at $V_{\mathrm{CB}} = 2\,V$. At this bias, carrier-induced excitonic resonance screening are eliminated and sharp excitonic absorption resonances are clearly observed in the photocurrent spectrum. Now, reverse bias results in the electric field increase within the QWs and an associated red shift of the absorption edge due to the QCSE. As a result, a positive signal is observed at the low-energy edge of the exciton resonance (1) and a negative signal is observed at the high-energy edge (2).

In Fig. 6(c), we compare between voltage modulation spectra as measured for various reverse bias levels of device C (similar results were obtained for device B, not shown). As clearly observed in Fig. 6(c), at low voltages the modulation spectrum is dominated by carrier-induced effects. At these voltages, the spectra are negative below the band edge and positive at the excitonic resonances due to carrier-induced bandgap reduction and exciton quenching. At higher voltages, the spectra are dominated by the QCSE.

Based on the voltage modulation signals interpretation, we can now explain the current induced results. The sharp negative signal observed in Fig. 5(b) at reverse bias of 1 V is due to the quenching of the excitonic absorption resonance as a result of carrier accumulation. In this case, the effects of voltage and current modulation are opposite since higher voltage depletes the wells while higher current increases the carrier concentration in the wells. The current modulation signals in Fig. 5(a) are more difficult to explain due to the large parasitic voltage modulations. Devices B and C have the same base and emitter structure
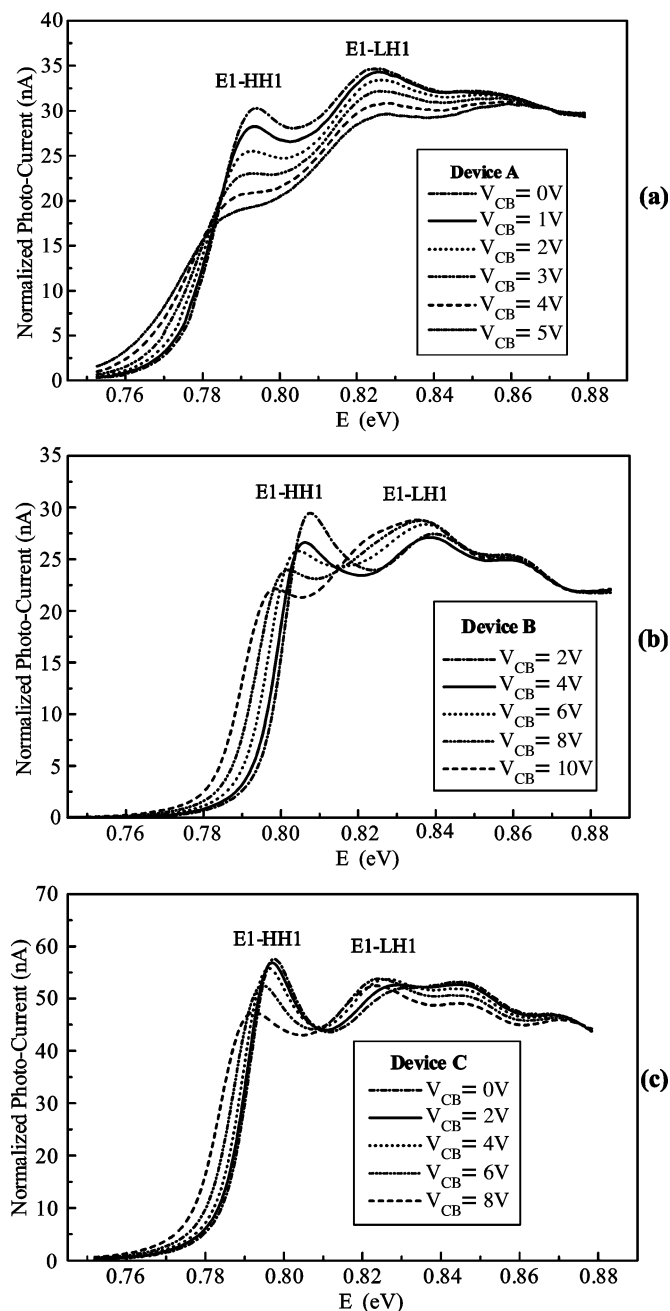
Fig. 4. Room-temperature photocurrent spectra measured at various bias levels. (a) The applied voltage quenched the excitonic absorption resonance in device A. Due to stronger confinement in devices (b) B and (c) C, the excitonic absorption resonance was observed at a wide reverse bias range.

Fig. 5. Comparison of the current- and voltage-induced absorption modulation spectra measured at 77 K for devices (a) B and (b) C. The amplitudes of the current modulation were 1 mA (~ 50 A/cm^2) and 20 μA(~ 1 A/cm^2) correspondingly. The voltage modulation amplitude was 400 mV for both devices.

and therefore similar current gain and lateral base layer resistance. The higher current used for measuring device B causes parasitic voltage modulation, which is 50 times larger than that in the measurements of device C. Decoupling of the current and voltage effects cannot be achieved by simple curve subtraction since the effective base collector voltage varies laterally across the device. Yet, the large signals that are observed for low voltages [Fig. 5(a)] and their reduction with the reverse dc bias increase indicate the strong influence of carrier accumulation on the absorption spectrum.

With this qualitative understanding, we try to more quantitatively estimate the effects of carrier injection on the absorption
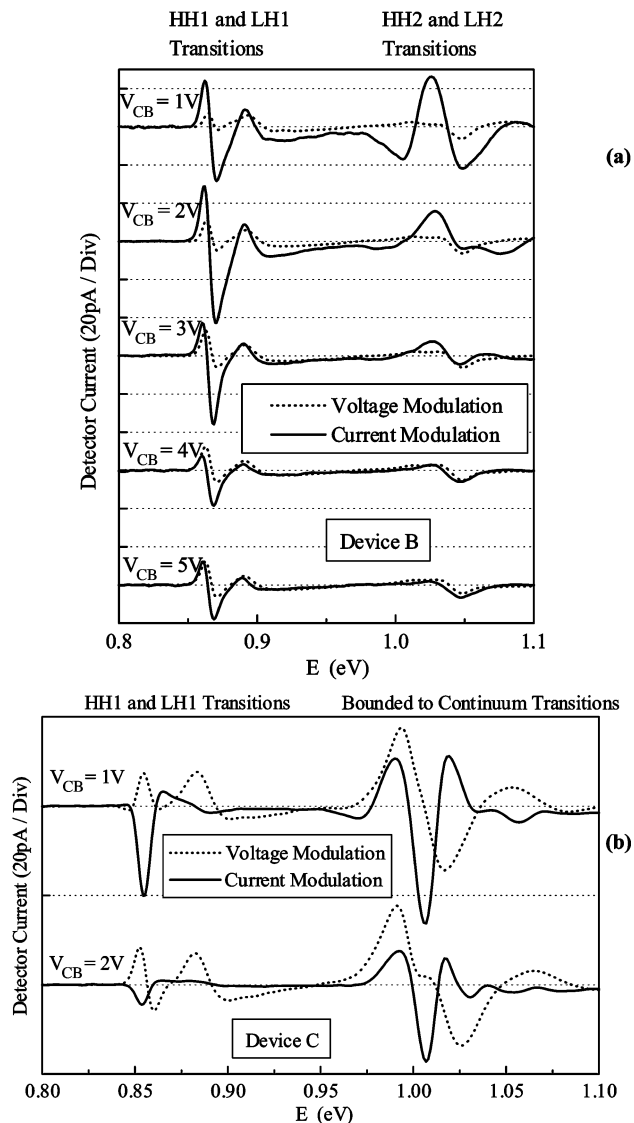
spectrum of the HBT modulators. The magnitude of the current-induced absorption modulation in Fig. 5(b) was evaluated by multiplying the voltage-induced absorption changes, extracted from photocurrent spectra, by the ratio of current and voltage modulation signal magnitudes. We found that a collector current of 20 μA(~ 1 A/cm^2) induced a relative absorption modulation of 15%. Higher collector currents yielded similar magnitudes, indicating effective saturation of the carrier density within the QWs.

We estimated the density of electrons required to generate this effect using eight-band $k \cdot p$ theory-based absorption calculations [14]–[16]. Our calculations indicate that saturation sheet density of 5×10^9 cm^{-2} electrons trapped in each QW is likely to produce the measured 15% absorption modulation.

We finally comment on the applicability of our approach for practical devices. Absorption modulation of 15% not is large enough for practical applications; moreover, this result was ob-
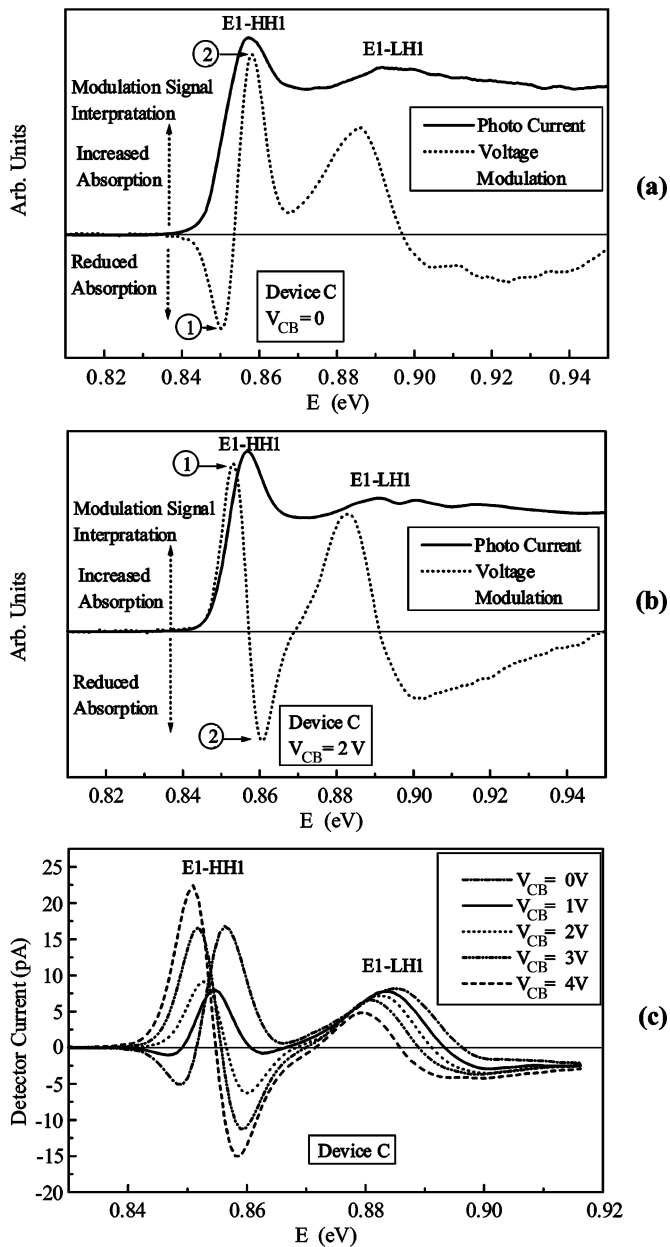
Fig. 6. Photocurrent and voltage modulation spectra measured at 77 K for device C at (a) $V_{CB} = 0$, (b) $V_{CB} = 2$ V, and (c) 400-mV voltage modulation spectra for various reverse biases. At low voltages, carrier-induced effects determine the absorption modulation characteristics. At high voltages, field-induced effects are dominant.

tained at a cryogenic temperature of 77 K. Further optimization is clearly needed for practical room-temperature operation.

The measured room-temperature current-induced modulation signals were too weak to analyze. Since excitonic absorption resonances are clearly observed at room temperature (photocurrent measurements in Fig. 4), we associated the weak signals with insufficient carrier accumulation. One way to enhance both trapping and confinement efficiency is by using higher barriers such as strained GaInP layers [17]. InGaAs wells can be used to form a strain-compensated lattice. The device efficiency could be further improved by using a waveguide configuration in which small changes in absorption and refractive index are sufficient for effective light modulation.

V. CONCLUSION

We studied the feasibility of light modulation by current injection. This was achieved by incorporating QW structures within the collectors of HBTs. Photocurrent and current-induced modulation spectroscopies were applied to measure the absorption modulation by the collector current. Current induced absorption modulation of 15% was obtained at 77 K. These results demonstrate the feasibility of light modulators, in which current injection, rather than electric field variation, controls the absorption spectrum.

ACKNOWLEDGMENT

REFERENCES

[1] D. A. B. Miller, "Quantum well electroabsorptive devices: physics and applications," in *Proc. 34th Scottish Universities Summer School in Physics*, 1988, pp. 71–93.

[2] S. Schmitt-Rink, D. S. Chemla, and D. A. B. Miller, "Linear and non linear optical properties of semiconductor quantum wells," *Adv. Phys.*, vol. 38, pp. 89–188, 1989.

[3] M. Wegener, T. Y. Chang, I. Bar-Joseph, J. M. Kuo, and D. S. Chemla, "Electroabsorption and refraction by electron transfer in asymmetric modulation doped multiple quantum well structures," *Appl. Phys. Lett.*, vol. 55, pp. 583–585, 1989.

[4] M. Wegener, J. E. Zucker, T. Y. Chang, N. J. Sauer, K. L. Jones, and D. S. Chemla, "Absorption and refraction spectroscopy of a tunable electron density quantum well and reservoir structure," *Phys. Rev. B*, vol. 41, pp. 3097–3104, 1990.

[5] J. E. Zucker, T. Y. Chang, M. Wegener, N. J. Sauer, K. L. Jones, and D. S. Chemla, "Large refractive index changes in tunable-electron-density InGaAs/InAlAs quantum wells," *IEEE Photon. Technol. Lett.*, vol. 2, pp. 29–31, Jan. 1990.

[6] J. E. Zucker, K. L. Jones, M. Wegener, T. Y. Chang, N. J. Sauer, M. D. Divino, and D. S. Chemla, "Multi gigahertz bandwidth intensity modulators using tunable electron density multiple quantum well waveguides," *Appl. Phys. Lett.*, vol. 59, pp. 201–203, 1991.

[7] R. A. Hamm, D. Ritter, and H. Temkin, "Compact metalorganic molecular beam epitaxy growth system," *J. Vac. Sci. Technol. A*, vol. 12, pp. 2790–2794, 1994.

[8] N. Shamir, D. Ritter, and C. Cytermann, "Beryllium doped InP/InGaAsP heterojunction bipolar transistors," *Solid State Electron.*, vol. 42, pp. 2039–2045, 1998.

[9] S. Fafard, E. Fortin, and A. P. Roth, "Oscillatory behavior of the continuum states in $In_xGa_{1-x}As/GaAs$ quantum wells due to capping-barrier layers of finite size," *Phys. Rev. B*, vol. 45, pp. 13 769–13 772, 1992.

[10] ——, "Effects of an electric field on the continuum energy levels in $In_xGa_{1-x}As/GaAs$ quantum wells terminated with thin cap layers," *Phys. Rev. B*, vol. 47, pp. 10 588–10 595, 1993.

[11] Y. H. Chen, C. H. Chan, and G. J. Jan, "Investigation of GaAs/AlGaAs multiple quantum well waveguides involving unconfined energy states," *J. Vac. Sci. Technol. B*, vol. 16, pp. 570–574, 1998.

[12] X. L. Zheng, D. Heiman, B. Lax, and F. A. Chambers, "Reflectance line shapes from GaAs/GaAlAs quantum well structures," *Appl. Phys. Lett.*, vol. 52, pp. 287–289, 1988.

[13] P. C. Klipstein and N. Apsley, "A theory for the electroreflectance spectra of quantum well structures," *J. Phys. C: Solid State Phys.*, vol. 19, pp. 6461–6478, 1986.

[14] G. A. Baraff and D. Gershoni, "Eigenfunction expansion method for solving the quantum wire problem," *Phys. Rev. B*, vol. 43, pp. 4011–4022, 1991.

[15] D. Gershoni, C. H. Henry, and G. A. Baraff, "Calculating the optical properties of multidimensional heterostructures: application to the modeling of quaternary quantum well lasers," *IEEE J. Quantum Electron.*, vol. 29, pp. 2433–2450, 1993.

[16] M. E. Pistol and D. Gershoni, "Modeling of electroabsorption in semiconductor quantum structures within the eight band theory," *Phys. Rev. B*, vol. 50, pp. 738–745, 1994.

[17] G. M. Cohen and D. Ritter, "Microwave performance of $Ga_xIn_{1-x}P/Ga_{0.47}In_{0.53}As$ resonant tunnelling diodes," *Electron. Lett.*, vol. 34, pp. 1267–1268, 1998.

Nachum Shamir received the B.Sc. degree in electrical engineering from the Technion, Israel Institute of Technology, Haifa, in 1988, the M.Sc. degree in electrical engineering from Tel Aviv University, Tel Aviv, Israel, in 1994, and the Ph.D. degree in electrical engineering from the Technion in 1999.

He served as an Adjunct Lecturer with the Technion Electrical Engineering faculty from 1998 to 2000. He joined the Mobile Platforms Group, Intel Israel, Haifa, in 1999. His current research and development areas are presilicon power estimation, analysis, and validation and post-silicon power and thermal characterization.

David Gershoni was born in Israel in 1953. He received the D.Sc. degree from the Technion, Israel Institute of Technology, Haifa, in 1986.

After receiving the D.Sc degree, he joined AT&T Bell Laboratories, Murray Hill, NJ, first as a postdoctorate and later as a Member of the Technical Staff. He joined the Department of Physics, Technion, in 1991. He has published more than 100 papers in international journals and has organized and lectured at major international conferences and workshops.

Dr. Gershoni was a recipient of the Fullbright Fellowship and the Wolf Prize.

Dan Ritter received the B.Sc, M.Sc., and Ph.D. degrees in electrical engineering from the Technion, Israel Institute of Technology, Haifa, in 1981, 1984, and 1989, respectively. He then carried out post-doctoral research during three years at AT&T Bell Laboratories, Murray Hill, NJ.

In 1992, he joined the Technion Electrical Engineering Department, where he is currently an Associate Professor. His main research interest is physics and the modeling of indium phosphide-based devices. His group has been using the metalorganic molecular beam epitaxy method to grow the epitaxial layers. The focus of his current activity is heterojunction bipolar transistors.